ISSN 0021-3640, JETP Letters, 2026, Vol. 124, No. 2, pp. 96–102. © The Author(s), 2026. This article is an open access publication.
Russian Text © The Author(s), 2026, published in Pis'ma v Zhurnal Eksperimental'noi i Teoreticheskoi Fiziki, 2026, Vol. 124, No. 2, pp. 106–113.

OPTICS AND LASER PHYSICS

Spatial Differentiation of Optical Signal Based on Fourier Filtering with Pixel and Gradient Metasurfaces

V. V. Yushkov[a], P. D. Kiryanov[a], A. S. Shorokhov[a], and A. A. Fedyanin[a,*]

[a] *Faculty of Physics, Moscow State University, Moscow, 119991 Russia*

**e-mail: fedyanin@nanolab.phys.msu.ru*

Received May 7, 2026; revised June 17, 2026; accepted June 17, 2026

Analog computations based on spatial Fourier filtering in a 4*f*-system enable the approaches of mathematical operations on images entirely optically, providing their pre-digital processing at high speed. Conventional implementations based on refractive elements are bulky and challenging from the standpoint of scalability. Due to efficient wavefront control, optical metasurfaces make it possible to replace such elements with planar nanostructures, ensuring compactness and subwavelength resolution in controlling the amplitude and phase of light. In this paper a comparison is carried out between pixel-based and gradient-based design approaches for optical metasurfaces based on gallium arsenide nanorings for spatial differentiation. In the pixel-based algorithm, each region of the metasurface (pixel) is considered as a square periodic lattice of identical nanoresonators. The gradient-based algorithm enables topology optimization by smoothly varying the size of nanorings across the metasurface. Despite the assumption that the gradient approach minimizes the artifacts inherent in pixel-based structures and ensures a more accurate matching with the required mathematical operation, the pixel structure demonstrates a Pearson correlation coefficient with the theoretical dependences that is 6–8% higher than that of the gradient structure.

DOI: 10.1134/S0021364026601624

1. INTRODUCTION

The development of analog optical computing is closely associated with the concept of spatial Fourier transformation. This common method is employed to solve tasks such as edge detection, correlation analysis, and denoising. The Fourier transform performed by a lens provides the decomposition of the electromagnetic field into a plane waves basis, thereby enabling the application of a range of linear operators to images without digitization [1–6]. This approach has not become widely used due to the large size of traditional optical components, as well as the challenges associated with scaling such systems up to industrial levels.

To overcome these limitations, it has been proposed to use two-dimensional arrays of nanostructured materials named metasurfaces capable of local modifying the parameters of incident electromagnetic radiation. Such devices are characterized by small thickness, compatibility with modern fabrication technologies, and the possibility of integration into photonic devices. Metasurfaces enable control over the wavefront, polarization, and spectrum at a thickness comparable to the wavelength of light [7–18]. This has enabled the development of compact elements for solving a wide range of optical problems, including the implementation of analog computations that realize operations such as differentiation, spatial frequency filtering, or convolution [4, 19–23].

Many previously demonstrated metasurfaces are based on a pixelized architecture [12, 24, 25], in which nanoresonators within a single pixel have identical shape and, consequently, the same optical response. Such structures possess a number of advantages; in particular, determining their response does not require a large amount of computational resources. However, such discretization leads to a stepwise profile of the phase and transmission function and, as a consequence, to a coarse approximation of continuous operators. Attempts to reduce the pixel size in order to improve approximation accuracy lead to changes in the response of each individual pixel due to a violation of periodicity and an increase in the contribution of boundary-induced artifacts to the resulting field. These factors significantly reduce the accuracy of analog operations.

To overcome the limitations, approaches to metasurface topology design based on numerical optimization methods and machine learning algorithms are currently being actively developed [26–29]. Such methods make it possible to account for the complex nonlinear relation between the shape parameters of nanoresonators and the transmission, reflection, and phase shift of light. At the same time, these methods have significant drawbacks. In particular, the optimization result often strongly depends on the definition of the initial point, and the optimization itself is local in nature, which complicates the search for a globally optimal solution. Moreover, full-structure simulation requires substantial time and computational resources; therefore, the practical implementation of such approaches is feasible only with the use of high-performance computing clusters.

An alternative approach is the gradient approach, in which the lattice period remains fixed while the shape of the resonator changes continuously. Gradient metasurfaces have demonstrated their effectiveness across a broad range of photonic applications. In nonlinear optics, gradient metasurfaces made it possible to realize optical harmonic generation over a wide spectral range [30] and to control the direction of nonlinear radiation [31]. In sensing applications, such structures have enabled the creation of multispectral platforms for the analyzing of biological samples, thereby opening the way to the development of portable devices for rapid diagnostics. In particular, gradient metasurfaces enable the analysis of molecular absorption bands [32], improve the results of IR spectroscopy [33], and determine nucleotide sequences [34]. In wavefront shaping applications, this principle underlies structures such as flat lenses [35], holographic elements [36], and devices for controlling the propagation direction of light beams [37]. From the point of analog optical computing, the gradient approach avoids the problems of pixel metasurfaces, in particular edge effects and limitations associated with low spatial resolution, thereby realizing a smooth complex transmission function of the structure. In addition, the continuous variation of shape parameters allows obtaining smooth and more fabrication-feasible structures, while also simplifying the incorporation of fabrication-related constraints. At the same time, this approach is more computationally efficient than methods that optimize the topology of the entire structure, which makes it promising for metasurface design problems.

This article compares the pixel-based and gradient-based approaches to the design of gallium arsenide-based metasurfaces for implementing spatial differentiation in a Fourier filtering scheme. In the pixel-based approach, the metasurface is divided into discrete regions (pixels), within each of them nanoresonators with identical shape parameters are used in a periodic array. The dependences of the transmission coefficient and phase shift on the topology of the nanoresonators for each individual pixel are obtained by the finite-difference time-domain (FDTD) method under periodic boundary conditions for a unit nanoparticle. The gradient-based approach is relying on the same dataset of transmission and phase data, although the periodicity conditions are violated as a result of the smooth variation of the shape parameters of the nanoresonators. The obtained data are approximated using a fully connected neural network to construct a smooth amplitude-phase dependence of the response on the shape parameters of the nanoresonators, after which the metasurface topology is determined using global stochastic optimization by the differential evolution method.

2. RESULTS

To implement fully optical differentiation of the input image along the x axis in a Fourier filtering setup, the input amplitude distribution $f(x,y)$ is placed in the front focal plane of the first lens, while the metasurface is positioned in the joint focal plane of the two lenses, which realize the complex transmission filtering $\hat{T}(u,v)$, where (u,v) denote the coordinates in the focal plane of the lenses (Fig. 1). The output field in the back focal plane of the second lens is determined by the relation

$$g(x,y) \propto \mathcal{F}\left[\hat{T}(u,v)\mathcal{F}\{f(x,y)\}\right], \tag{1}$$

where $\mathcal{F}$ denotes the forward Fourier transform performed by the lens. To perform differentiation in this scheme, the transmission function is

$$\hat{T}(u,v) = T_0(u,v)e^{i\Delta\varphi_0(u,v)} \propto |u|e^{i\,\mathrm{sgn}(u)\pi/2}, \tag{2}$$

subject to $T_0 \leq 1$ and the finite size of the structure. The field at the output of the system will be the derivative of the input field distribution inverted with respect to the principal optical axis of the lens:

$$g(x,y) \propto \frac{\partial f(-x,-y)}{\partial x}. \tag{3}$$

The metasurface with a size of $D = 110$ μm is a square lattice of unit cells with a period a. The nanoresonators have a ring shape with an outer diameter d and an inner diameter b, a height of $h = 150$ nm, and are embedded in SiO_2. This shape is subject to less deformation during fabrication than rectangular designs, and at the same time has two independent degrees of freedom (inner and outer diameters), which allows for more precise tuning of optical characteristics compared to discs.

For the determination of the metasurface topology, a dataset of complex transmission coefficients was obtained:

$$\hat{T}(a,d,b) = T(a,d,b)e^{i\Delta\varphi(a,d,b)}, \tag{4}$$

where $T(a,d,b)$ and $\Delta\varphi(a,d,b)$ are the transmission and the phase shift of the transmitted wave, respectively. The dependences $T(a,d,b)$ and $\Delta\varphi(a,d,b)$ were calculated using the FDTD method for a single unit cell with a period $a \in [300, 550]$ nm, modeled as part of an infinite square array of nanoring resonators with outer diameter $d \in [250, 400]$ nm, and inner diameter $b \in [0, 250]$ nm, using periodic boundary conditions. This approach corresponds to the local periodicity approximation and substantially reduces the computational cost of obtaining a dataset of the periodic

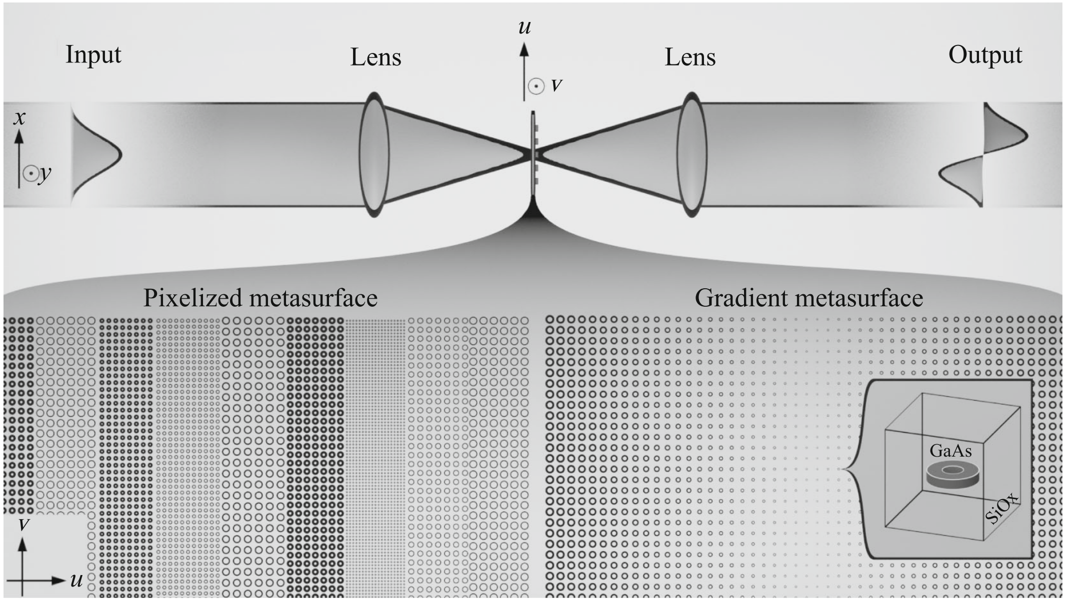

Fig. 1. Optical setup of Fourier filtering is a 4*f* system: the metasurface is positioned at the focal plane of both lenses, the input image is located in the front focal plane of the first lens, and the output image is detected in the back focal plane of the second lens. Two types of metasurfaces are used for filtering: a pixelized one (shown at the bottom left) and a gradient one (at the bottom right). Both metasurfaces consist of GaAs nanorings of varying size, as illustrated in the insert on the right.

array of nanoresonators response required for the subsequent optimization of the metasurface topology.

Two-dimensional cross sections of the transmission T and the phase shift, plotted in the (a,d) and (d,b) planes for fixed values of $b = 0$ nm and $a =$ 545 nm, respectively, are shown in Fig. 2. Resonant features in the transmission and phase shift spectra are a result of the excitation of Mie-type resonances in the nanorings. The transmission has minima caused by spectral overlap of the electric dipole (ED), electric quadrupole (EQ), magnetic dipole (MD), and magnetic quadrupole (MQ) resonant modes. A small variation in the shape of the nanoresonator causes the phase shift to change sharply by values up to 2π. As the hole size in the rings increases, the coincident resonant modes split into pairs of ED+MQ and MD+EQ, resulting in the appearance of two diverging low-pass branches and the absence of the 2π phase shift. The resulting resonance dependences make it possible to implement a wide range of switchable amplitude-phase Fourier filters.

To obtain an approximation of $T(a,d,b)$ and $\Delta\varphi(a,d,b)$, two regression models were trained in PyTorch for the transmission T and the phase shift $\Delta\varphi(x)$. The output vector of the neural network was formed from the pair $(\cos\Delta\varphi, \sin\Delta\varphi)$, as a result of which the output vector was insensitive to phase differences on the edges of range $[0, 2\pi]$. The input vector was linearly scaled to the range $[-1, 1]$. The training dataset of 240 thousand rows was divided into training and test sets in a 3:1 ratio. The training set was used to optimize the model parameters, while the test set was used only to control the quality of training. The training dataset was divided into batches with 512 rows for transmission and 1024 rows for phase shift, and at each step a forward pass through the batch, loss computation, backpropagation, and weight update were performed. The Adam optimizer with a learning rate of 10^{-3} was used for parameter updating, and the mean squared error (MSE) was employed as the performance criterion. As a result of training over 500 epochs, RMSE values of 0.16 for transmission and 0.23 for phase were obtained on the test datasets, which confirms sufficient approximation accuracy for the use of the model in the inverse problem of metasurface topology optimization.

The inverse problem was formulated as the search for a set of shape parameters that provide proximity between the predicted values $(T, \Delta\varphi)$ and the target profiles $(T_0, \Delta\varphi_0)$. In addition to the constraints set by the boundaries of the calculated parameters a, d and b, data rows satisfying the conditions $a < d + 50$ nm and $d < b + 50$ nm, were excluded from further consideration. This is caused by the technological limitations of electron-beam lithography, which is used to fabricate such type of nanoresonators.

Additional global parameters were used in the optimization: the overall phase shift $\Delta\varphi_z$ and the scaling factor $t_z \in [0.7, 1.0]$, which were optimized jointly with the shape parameters. The overall phase shift $\Delta\varphi_z$ was introduced to account for the uncertainty in the initial phase of the wave.

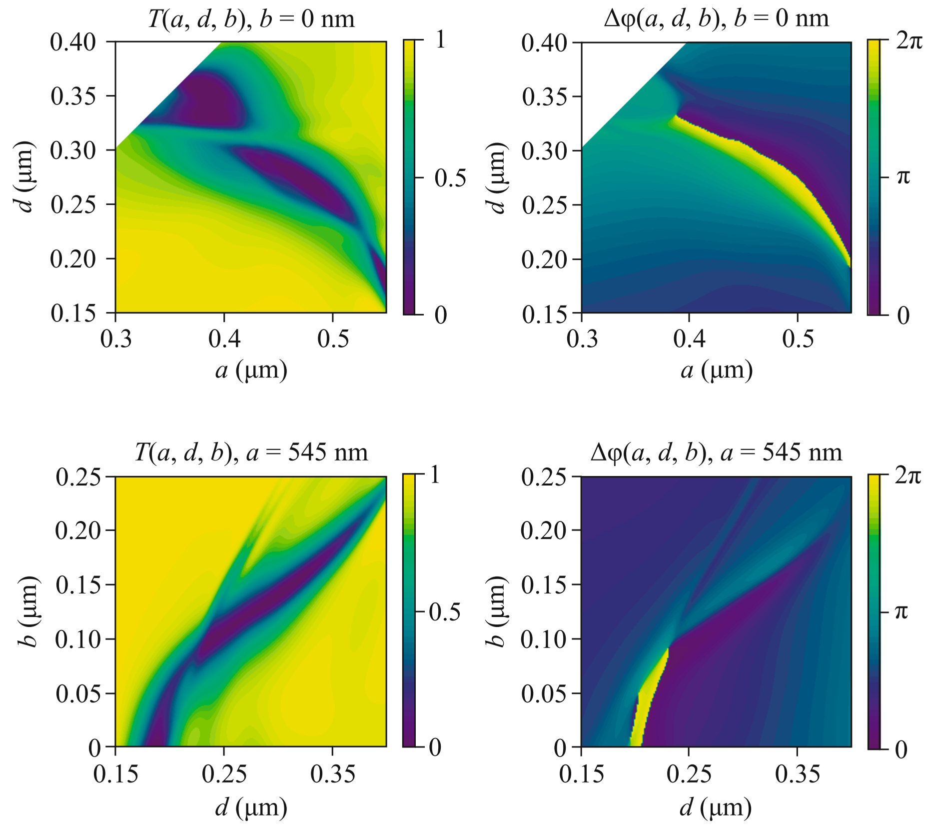

Fig. 2. (Color online) Transmission T and phase shift $\Delta\varphi$ of the metasurface as functions of the outer diameter d of the nanorings, their inner diameter b, and the lattice period a, obtained using a neural-network model trained on the results of FDTD simulations. Top row: dependence on the period a and diameter d for GaAs nanodisks. Bottom row: dependence on the inner diameter b and outer diameter d for metasurfaces with a fixed lattice period $a = 545$ nm.

The function Δ, minimized in the $2N + 3$-dimensional space $(a, d_1, \ldots, d_N, b_1, \ldots, b_N, \varphi_z, t_z)$, was defined as

$$\Delta = \sum_{i=1}^{N} (T(a,d_i,b_i))^2 + (t_z T_0(u_i))^2 - 2T(a,d_i,b_i) t_z T_0(u_i) \times \cos(\Delta\varphi(a,d_i,b_i) - \Delta\varphi_0(u_i) - \Delta\varphi_z)). \quad (5)$$

Here, $u_i = \frac{x}{D}(i + 1 - [N/2])$, [...] is the integer part, D is the size of the metasurface. Optimization was performed using the differential evolution method for $N = 11$ on a sampled set of 200 points over 5000 iterations. Next, based on the optimized period a, the number of nanoresonators in the metasurface was determined, after which the values of d and b for all nanoresonators were determined using linear interpolation. The optimization results are shown in Fig. 3. The red points, corresponding to the optimized shape of the nanoresonators at a given coordinate u, partially coincide with the theoretical dependence $\hat{T}(u,v)$, marked by the black curve. The blue curve indicates the transmission and phase shift values corresponding to the pixel metasurface. The deviations in the central part of the plot at low transmission values are caused by the optimization function, in which values with lower transmitted light field amplitudes are given less weight during optimization.

To verify the optimization results, a full-wave FDTD simulation was performed to model the propagation of a Gaussian light beam with a width of 1.23 mm (Fig. 4, gray dashed curve) through the optimized gradient metasurface at a wavelength of $\lambda = 850$ nm for two linear polarizations: along the x axis and along the y axis. At the output of the 4f system, the distribution of the square of the field magnitude $|E_{\text{out}}(x)|^2$, which, for a differentiation operation, should reproduce the square of the modulus of the derivative of the input field, i.e., have a distinctive double-lobed shape for a Gaussian input beam (Fig. 4, gray solid curve). The quantitative agreement of the simulation results with the theoretical dependence was estimated by the Pearson correlation coefficient between the normalized cross-sectional areas of the square of the electric field magnitude in the output images. For comparison with traditional approach, a pixel-based metasurface was

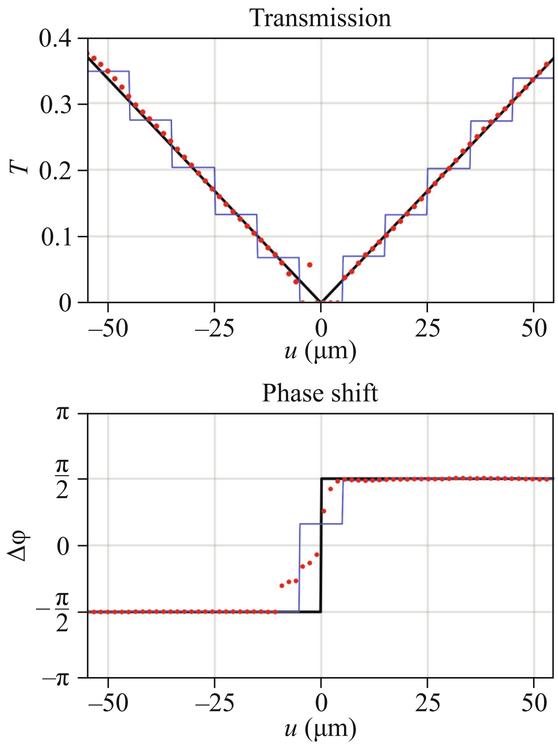

Fig. 3. (Color online) (Black curve) Theoretical and (red circles) optimized (top panel) transmission coefficient and (bottom panel) phase shift versus the coordinate of the metasurface. The blue curve indicates the transmission coefficient and phase shift for the corresponding pixel metasurface.

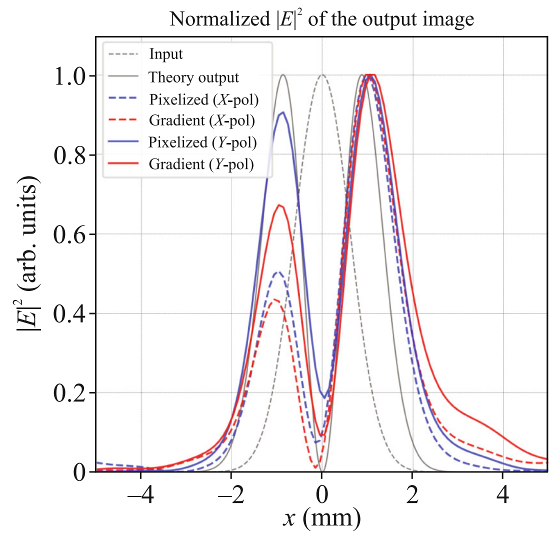

Fig. 4. (Color online) Cross section of the square of the electric field magnitude of the output image after processing by the (red curve) gradient and (blue curve) pixel metasurfaces, respectively, compared to the (gray solid curve) required theoretical dependence. The square of the electric field magnitude of the input image is indicated by the gray dashed curve. The values are normalized to the maximum $|E|^2$ of each curve.

modeled in which the nanoresonators within a single pixel are identical, and the required transfer function is approximated by a step profile (see Fig. 3, blue curve). Similar nanorings were used as resonators in the pixel implementation, and optimization was performed for the parameters a, d, and b within the same ranges.

A full-wave FDTD calculation for a gradient metasurface with x-polarized wave shows a correlation coefficient of 82% with the theoretical dependence, while for a pixel metasurface, it is 88%. Under the same conditions for y-polarized wave, these values are 87 and 95% for the gradient and pixel metasurfaces, respectively. Cross sections of the resulting $|E|^2$ distributions along the x axis are shown in Fig. 4: solid curves correspond to y-polarization, dashed curves to x-polarization; red curves correspond to the gradient metasurface, blue curves to the pixel metasurface.

Despite the noticeable difference between the pixel-based transmission function and a smooth gradient-based function, the discretization of the Fourier filter did not result in any significant distortion of the final field distribution. Moreover, for both polarizations, the gradient metasurface exhibited a lower correlation coefficient than the pixel-based one. This is due to the fact that, in this case, the gradient of the shape parameters was quite large: for the gradient metasurface, this led to a significant violation of the periodicity conditions and, consequently, to great variation of the response. In the pixel metasurface, by contrast, the optical response was determined by strictly periodic conditions, and despite the pixel size limitation, the resulting field distribution exhibited a higher level of correlation.

In the case of y-polarized light, the correlation coefficient between the calculated and theoretical field distributions is higher than for x-polarized light. This is because for y-polarized light the direction of the field vector E coincides with the direction along which the periodicity of both the pixel gradient structures is preserved. As a result, the translational symmetry of the field along this direction remains invariant. For x-polarization, which is perpendicular to the direction of periodicity preservation, the local field between nanoparticles in a gradient metasurface varies with changes in the parameters of the surrounding nanoresonator shape, whereas in a pixel metasurface, it changes abruptly at pixel edges. The change in the local field occurring along the direction of the periodicity break leads to a distortion of the metasurface's amplitude-phase profile and a decrease in the correlation coefficient.

3. CONCLUSIONS

An approach is proposed for designing a gradient metasurface based on gallium arsenide nanoring resonators to implement spatial optical differentiation in a 4*f*-system Fourier filtering scheme. It is shown that the use of a dataset of periodic cell response, a neural network approximation, and optimization via the differential evolution method allows for the creation of an amplitude-phase profile close to the target transfer function. The results of full-wave simulations demonstrate that, within the scope of this problem, the gradient metasurface is less accurate than the pixel-based metasurface in performing mathematical operations. A decrease in the correlation coefficient is observed for both linear polarizations of the incident radiation and is explained by the fact that, at large gradients of shape parameters, the applicability of the local periodicity approximation is disrupted. A dependence of the accuracy of the operation on the uniformity of the near-field distribution, caused by different polarization directions of the incident light, has been identified. The results show the limitations of the quasi-periodic approach in the synthesis of gradient metasurfaces for analog optical computing tasks.

FUNDING

This work was supported by the Russian Science Foundation, project no. 25-12-00355, https://rscf.ru/project/25-12-00355/. We are grateful the Noncommercial Foundation for Support of Science and Education INTELLECT. V.V. Yushkov acknowledges the support of the Theoretical Physics and Mathematics Advancement Foundation BASIS.

CONFLICT OF INTEREST

The authors of this work declare that they have no conflicts of interest.

OPEN ACCESS

REFERENCES

1. A. V. Lugt, "Signal detection by complex spatial filtering," IEEE Trans. Inf. Theory **10**, 139 (1964).
2. O. Bryngdahl, "Geometrical transformations in optics," J. Opt. Soc. Am. **64**, 1092 (1974).
3. J. Goodman, *Introduction to Fourier Optics* (Macmillan Learning, New York, 2017).
4. T. Manzur, J. Zeller, and S. Serati, "Optical correlator based target detection, recognition, classification, and tracking," Appl. Opt. **51**, 4976 (2012).
5. A. D. Gartman, A. S. Ustinov, A. S. Shorokhov, and A. A. Fedyanin, "Spatial separation of scalar light beams with orbital angular momentum using a phase metasurface," JETP Lett. **114**, 441 (2021).
6. P. A. Khorin, N. A. Ivliev, and S. N. Khonina, "Optical spatial filters for controlling the width of extracted object edges," J. Opt. Technol. **92**, 280 (2025).
7. I. Staude, A. E. Miroshnichenko, M. Decker, N. T. Fofang, S. Liu, E. Gonzales, J. Dominguez, T. S. Luk, D. N. Neshev, I. Brener, and Y. Kivshar, "Tailoring directional scattering through magnetic and electric resonances in subwavelength silicon nanodisks," ACS Nano **7**, 7824 (2013).
8. N. Yu and F. Capasso, "Flat optics with designer metasurfaces," Nat. Mater. **13**, 139 (2014).
9. Y. F. Yu, A. Y. Zhu, R. Paniagua-Domínguez, Y. H. Fu, B. Luk'yanchuk, and A. I. Kuznetsov, "High-transmission dielectric metasurface with 2π phase control at visible wavelengths," Laser Photon. Rev. **9**, 412 (2015).
10. M. Decker, I. Staude, M. Falkner, J. Domínguez, D. N. Neshev, I. Brener, T. Pertsch, and Y. S. Kivshar, "High-efficiency dielectric Huygens' surfaces," Adv. Opt. Mater. **3**, 813 (2015).
11. A. I. Kuznetsov, A. E. Miroshnichenko, M. L. Brongersma, Y. S. Kivshar, and B. Luk'yanchuk, "Optically resonant dielectric nanostructures," Science **354**, aag2472 (2016).
12. K. E. Chong, L. Wang, I. Staude, A. R. James, J. Domínguez, S. Liu, G. S. Subramania, M. Decker, D. N. Neshev, I. Brener, and Y. S. Kivshar, "Efficient polarization-insensitive complex wavefront control using Huygens' metasurfaces based on dielectric resonant meta-atoms," ACS Photon. **3**, 514 (2016).
13. P. Genevet, F. Capasso, F. Aieta, M. Khorasaninejad, and R. Devlin, "Recent advances in planar optics: From plasmonic to dielectric metasurfaces," Optica **4**, 139 (2017).
14. A. C. Overvig, S. Shrestha, S. C. Malek, M. Lu, A. Stein, C. Zheng, and N. Yu, "Dielectric metasurfaces for complete and independent control of the optical amplitude and phase," Light Sci. Appl. **8**, 92 (2019).
15. A. V. Konovalova, A. A. Popkova, T. G. Baluian, and A. A. Fedyanin, "Design features of optical diffraction neural networks," JETP Lett. **123**, 85 (2026).
16. A. I. Musorin, A. S. Shorokhov, A. A. Chezhegov, T. G. Baluyan, K. R. Safronov, A. V. Chetvertukhin, A. A. Grunin, and A. A. Fedyanin, "Photonics approaches to the implementation of neuromorphic computing," Phys. Usp. **193**, 1284 (2023).
17. D. N. Neshev and A. E. Miroshnichenko, "Enabling smart vision with metasurfaces," Nat. Photon. **17**, 26 (2023).
18. A. I. Kuznetsov, M. L. Brongersma, J. Yao, et al., "Roadmap for optical metasurfaces," ACS Photonics **11**, 816 (2024).

19. M. S. Monjur, S. Tseng, R. Tripathi, J. J. Donoghue, and M. S. Shahriar, "Hybrid optoelectronic correlator architecture for shift-invariant target recognition," J. Opt. Soc. Am. A **31**, 41 (2014).
20. A. Chizari, S. Abdollahramezani, M. V. Jamali, and J. A. Salehi, "Analog optical computing based on a dielectric meta-reflect array," Opt. Lett. **41**, 3451 (2016).
21. J. Zhou, S. Liu, H. Qian, Y. Li, H. Luo, S. Wen, Z. Zhou, G. Guo, B. Shi, and Z. Liu, "Metasurface enabled quantum edge detection," Sci. Adv. **6**, eabc4385 (2020).
22. V. V. Yushkov, V. A. Sitnyansky, A. S. Shorokhov, and A. A. Fedyanin, "Analog optical correlation augmented by Mie-resonant metasurfaces," ACS Photonics **11**, 2506 (2024).
23. V. V. Yushkov, A. S. Shorokhov, and A. A. Fedyanin, "Ultrafast optically tunable GaAs metasurfaces for analog image processing," ACS Omega **11**, 3311 (2026).
24. K. E. Chong, I. Staude, A. James, J. Dominguez, S. Liu, S. Campione, G. S. Subramania, T. S. Luk, M. Decker, D. N. Neshev, I. Brener, and Y. S. Kivshar, "Polarization-independent silicon metadevices for efficient optical wavefront control," Nano Lett. **15**, 5369 (2015).
25. M. Cotrufo, S. Singh, A. Arora, A. Majewski, and A. Alù, "Polarization imaging and edge detection with image-processing metasurfaces," Optica **10**, 1331 (2023).
26. J. Jiang and J. A. Fan, "Global optimization of dielectric metasurfaces using a physics-driven neural network," Nano Lett. **19**, 5366 (2019).
27. G. A. Kolosov, A. S. Shorokhov, and A. A. Fedyanin, "Numerical simulation of a photonic tensor core for the hardware acceleration of the optical matrix-vector multiplication," JETP Lett. **120**, 932 (2024).
28. S. Jafar-Zanjani, S. Inampudi, and H. Mosallaei, "Adaptive genetic algorithm for optical metasurfaces design," Sci. Rep. **8**, 11040 (2018).
29. G. Kolosov, E. Kabak, A. Shorokhov, and A. Fedyanin, "Reconfigurable mode converters based on low-loss phase change materials for integrated optical computing," Opt. Express **34**, 8087 (2026).
30. P. Jangid, F. U. Richter, M. L. Tseng, I. Sinev, S. Kruk, H. Altug, and Y. Kivshar, "Spectral tuning of high-harmonic generation with resonance-gradient metasurfaces," Adv. Mater. **36**, 2307494 (2023).
31. L. Wang, S. Kruk, K. Koshelev, I. Kravchenko, B. Luther-Davies, and Y. Kivshar, "Nonlinear wavefront control with all-dielectric metasurfaces," Nano Lett. **18**, 3978 (2018).
32. F. U. Richter, I. Sinev, S. Zhou, A. Leitis, S. Oh, M. L. Tseng, Y. Kivshar, and H. Altug, "Gradient high-Q dielectric metasurfaces for broadband sensing and control of vibrational light–matter coupling," Adv. Mater. **36**, 2314279 (2024).
33. I. Sinev, A. Cargioli, D. Piciocchi, F. U. Brikh, J. Faist, and H. Altug, "Metasurface-enhanced midinfrared imaging spectroscopy with broadband quantum cascade lasers," Nat. Commun. **17**, 7045 (2026).
34. H. Feng, S. Min, S. Xuan, Z. Gan, Z. Sun, Y. Gao, S. Yang, W.-D. Li, and Y. Chen, "Gradient nanoplasmonic imaging metasurface for rapid and label-free detection of SARS-CoV-2 sequences," Talanta **278**, 126533 (2024).
35. M. Khorasaninejad and F. Capasso, "Metalenses: Versatile multifunctional photonic components," Science **358**, eaam8100 (2017).
36. G.-Y. Lee, G. Yoon, S.-Y. Lee, H. Yun, J. Cho, K. Lee, H. Kim, J. Rho, and B. Lee, "Complete amplitude and phase control of light using broadband holographic metasurfaces," Nanoscale **10**, 4237 (2018).
37. F. He, K. F. MacDonald, and X. Fang, "Continuous beam steering by coherent light-by-light control of dielectric metasurface phase gradient," Opt. Express **28**, 30107 (2020).

Translated by the authors